Molecular Biology of the Cell
Vol. 20, 780–790, February 1, 2009

Early Stages of Golgi Vesicle and Tubule Formation Require Diacylglycerol

Lennart Asp,* Fredrik Kartberg,* Julia Fernandez-Rodriguez,† Maria Smedh,† Markus Elsner,* Frederic Laporte,‡ Montserrat Bárcena,§ Karen A. Jansen,§ Jack A. Valentijn,§ Abraham J. Koster,§ John J.M. Bergeron,‡ and Tommy Nilsson*

*Department of Medical and Clinical Genetics and †Centre for Cellular Imaging, the Sahlgrenska Academy at the University of Gothenburg, 405 30 Gothenburg, Sweden; ‡Department of Anatomy and Cell Biology, McGill University, Montreal, Quebec, H3A 2B2 Canada; and §Department of Molecular Cell Biology (MCB-EM), Leiden University Medical Center, 2333 ZC Leiden, The Netherlands

Submitted March 10, 2008; Revised November 13, 2008; Accepted November 17, 2008
Monitoring Editor: Sean Munro

We have investigated the role for diacylglycerol (DAG) in membrane bud formation in the Golgi apparatus. Addition of propranolol to specifically inhibit phosphatidate phosphohydrolase (PAP), an enzyme responsible for converting phosphatidic acid into DAG, effectively prevents formation of membrane buds. The effect of PAP inhibition on Golgi membranes is rapid and occurs within 3 min. Removal of the PAP inhibitor then results in a rapid burst of buds, vesicles, and tubules that peaks within 2 min. The inability to form buds in the presence of propranolol does not appear to be correlated with a loss of ARFGAP1 from Golgi membranes, as knockdown of ARFGAP1 by RNA interference has little or no effect on actual bud formation. Rather, knockdown of ARFGAP1 results in an increase in membrane buds and a decrease of vesicles and tubules suggesting it functions in the late stages of scission. How DAG promotes bud formation is discussed.

INTRODUCTION

Formation of buds to generate intracellular transport vesicles from membranes such as Golgi cisternae involves both coat binding and local lipid conversion (for reviews and theoretical models, see Kirchhausen, 2000; Shemesh *et al.*, 2003; Weiss and Nilsson, 2003; Bethune *et al.*, 2006). For COPI vesicles, formation of buds is initiated by the small GTPase ARF1 (ADP-ribosylation factor 1) which, in its GTP-conferred conformation, drives coatomer recruitment from the cytosol to both Golgi and pre-Golgi membranes (Palmer *et al.*, 1993). Indeed, ARF1 and coatomer are sufficient for both bud and vesicle formation as evidenced in in vitro experiments using liposomes forming coated vesicles in a controlled manner (Spang *et al.*, 1998). Addition of ARFGAP1, a GTPase-activating protein for ARF1, then yielded uncoated vesicles of the expected size of ~50–60 nm in diameter (Reinhard *et al.*, 2003).

The situation in biological membranes is likely more refined involving additional as well as alternative components to promote or prevent vesicle formation such that Golgi function is maintained. Here, both ARF1 and ARFGAP1 have been implicated in vesicle formation through direct or indirect modulation of lipid synthesis such that bud formation and membrane fission are promoted. For example, ARF1 stimulates the production of phosphatidic acid (PA) from phosphatidylcholine (PC; Brown *et al.*, 1993; Cockcroft *et al.*, 1994) through the activation of phospholipase D (PLD) in a nucleotide (GTP)-specific manner (Brown *et al.*, 1995; Houle *et al.*, 1995; Ktistakis *et al.*, 1995). Such ARF1-mediated PLD stimulation results in an increased vesicle production (Ktistakis *et al.*, 1996; Chen *et al.*, 1997). This ability of ARF1 to stimulate lipid formation in the Golgi apparatus offers a possibility to mechanistically link lipid conversion with coat recruitment. PA may also be converted to diacylglycerol (DAG) and the ratio between DAG and PC seems to influence protein transport through the Golgi apparatus in yeast (Rivas *et al.*, 1999). PA can also be synthesized from lysophosphatidic acid (LPA) by a LPA acyltransferase–dependent pathway through acyl-CoA and in fact, inhibitor studies indicate that this pathway is required for COPI vesicle formation (Ostermann *et al.*, 1993; Yang *et al.*, 2005).

Theoretical models predict that formation of PA is required for the formation of vesicle buds such that this cone-shaped lipid enables the formation of negative curvature in the cytosolic leaflet of the lipid bilayer (for a theoretical model, see Shemesh *et al.*, 2003 and references therein). Likewise, conversion of PA into LPA, an inverted cone-shaped lipid, is thought to allow for the formation of positive curvature needed for outward bending of the lipid bilayer to form the bud. Indeed, addition of an inhibitor that prevents the formation of LPA from PA effectively inhibits retrograde transport between the Golgi apparatus and the endoplasmic reticulum (ER), in vivo (de Figueiredo *et al.*, 2000). The experimental evidence for a requirement of PA to form negative curvature in the Golgi is mostly based on work examining CtBP/Bars-50 (Schmidt *et al.*, 1999; Weigert *et al.*, 1999). As this protein lacks enzymatic activity (Gallop

This article was published online ahead of print in *MBC in Press* (http://www.molbiolcell.org/cgi/doi/10.1091/mbc.E08–03–0256) on November 26, 2008.

Address correspondence to: Tommy Nilsson (tommy.nilsson@gu.se).

et al., 2005), CtBP/Bars-50 is thought to promote COPI vesicle formation at the stage of vesicle budding through interaction with ARFGAP1, an interaction that is enhanced by acyl-CoA but inhibited by NADH, where the latter is competing with the binding of acyl-CoA to the Rossman fold of CtBP/Bars-50. Thus CtBP/Bars-50 seems to have an important role for ARFGAP1 function by regulating its ability to stimulate fission (Yang *et al.*, 2005), possibly by modulating the ability of ARFGAP1 to bind to Golgi membranes via its ALPS domain (Corda *et al.*, 2006). CTBP/Bars-50 might also stimulate bud formation and tubulation directly by binding to PA (Yang *et al.*, 2008). Furthermore, PA can be converted to DAG through dephosphorylation of PA. This enzymatic step is mediated by phosphatidate phosphohydrolases (PAPs) and is effectively inhibited by the pharmaceutical agent, propranolol (proPr). This agent inhibits the activity of the two known classes of phosphohydrolase activities (type 1 and 2; Roberts *et al.*, 1998). The inhibition of PAP affects the production of DAG but also the subsequent synthesis of PC, phosphatidylethanolamine, and triacylglycerol (Truett *et al.*, 1992). ProPr has been used previously to highlight the importance of DAG in the recruitment of proteins containing a DAG-binding domain C1 (as in protein kinase D [PKD]), to *trans*-Golgi membranes (Baron and Malhotra, 2002; Carrasco and Merida, 2004, 2007). Inhibition of PAP enzymes by proPr affects the ability of PKD being recruited to Golgi membranes such that formation of transport carriers at the *trans*-side of the Golgi apparatus is impaired (Baron and Malhotra, 2002). This inhibition in vesicle formation exists partially at the level of PA to DAG conversion and, as was recently shown, partially at the level of peri-Golgi vesicles (Fernandez-Ulibarri *et al.*, 2007; Sonoda *et al.*, 2007). Here, inhibition of PAP by proPr resulted in the inability to form vesicles. In the Fernandez-Ulibarri *et al.* (2007) study, this inability appeared at the stage of membrane fission and was explained by a concurrent and partial loss of ARFGAP1 from Golgi membranes. In this study, we show that the primary effect of DAG is at the point of bud formation whereas ARFGAP1 is needed at later stages such as fission.

MATERIALS AND METHODS

Reagents

Antipain aprotinin, apyrase benzamidine, GTP, leupeptin, pepstatin, PMSF, proPr, *N*-ethylmalemide polyvinylpyrrolidone (PVP-40T), soybean trypsin inhibitor, phosphate-buffered saline (PBS)-Tween (0,05%) were from Sigma-Aldrich (Stockholm, Sweden) and Biomax X-Omat XAR or MR films from Eastman Kodak (Rochester, NY). ATP, creatine phosphate, and creatine kinase were from Roche AB (Stockholm, Sweden). 1,4-Dithiothreitol was from Biomol (Hamburg, Germany). ECL detection kit was from GE Healthcare Bio-Sciences AB (Uppsala, Sweden). Thirty percent (wt/vol) acrylamide/0.8% (wt/vol) bis-acrylamide solution was from Bio-Rad (Sundbyberg, Sweden). Uranyl acetate, glutaraldehyde, and glycerol were from E. Merck (Stockholm, Sweden). Osmium tetroxide was from Agar Scientific (Essex, United Kingdom). Protran nitrocellulose membranes (0.45 μm) were from Schleicher & Schuell (Dassel, Germany). Minimum essential medium (MEM), fetal bovine serum (FBS), glutamine, and Lipofectamine RNAiMAX and Lipofectamine 2000 were purchased from Invitrogen (Carlsbad, CA).

Antibodies, Cytosol, Membrane, and In Vitro Binding

Rabbit polyclonal antibodies to ARFGAP1 have been described previously (Lanoix *et al.*, 2001) as have monoclonal antibodies to native coatomer, CM1A10 (Palmer *et al.*, 1993) and βCOP, M3A5 (Allan and Kreis, 1986). HRP-labeled polyclonal antibodies to rabbit and mouse IgG were purchased from Dianova (Hamburg, Germany). Full-length His-ARFGAP1 was purified as described before (Huber *et al.*, 2001). Purified rat liver Golgi membranes and rat liver cytosol were prepared and treated as described (Lanoix *et al.*, 1999). Typically, membranes were purified ~100-fold over that of the homogenate. The in vitro binding assay was performed under in vitro budding conditions as described (Lanoix *et al.*, 2001) in a final volume of 200 μl. The standard assay mixture contained 100 μg of Golgi membranes, 5 mg/ml rat liver cytosol, an ATP-regenerating system (1 mM ATP, 5 mM creatine phosphate, and 10 U/ml creatine kinase), 1 mM DTT, a protease inhibitor cocktail and 0.5 mM GTP.

Cell Culture and Transfection

HeLa cells were grown in MEM supplemented with 10% FBS, penicillin (100 U/ml), streptomycin (100 μg/ml), and L-glutamine (2 mM). Cells expressing ARFGAP1^{EGFP} were grown in the presence of 200 μg/ml geneticin (G-418). Small interfering RNA (siRNA) constructs against ARFGAP1 and green fluorescent protein (GFP; mock) were custom synthesized by Invitrogen using published sequences (Frigerio *et al.*, 2007). In Supplementary Figure 5B, a negative control sequence purchased from MWG Eurofins Operon (Ebersberg, Germany), (5′-AGGUAGUGUAAUCGCCUUG-3′) was used (scambled). ARFGAP-YFP and PKD-K618N were kindly provided by Dr. J. Lippincott-Schwartz (National Institutes of Health, Bethesda, MD) and Dr. Malhotra (Cell and Development Program, Centro de Regulacion Genomica, Barcelona, Spain). Transfections were performed with Lipofectamine RNAiMax following the manufacturer's instructions (Invitrogen). The medium containing the transfection reagent was replaced by fresh medium 24 h after transfection. This did not affect the degree of RNA silencing but greatly improved the overall ultrastructural morphology of intracellular membranes as deduced by electron microscopy.

Light and Electron Microscopy

Indirect immunofluorescence on fixed cells was performed as described (Dominguez *et al.*, 1998). Imaging of living cells was performed as follows: HeLa cells stably expressing GalNAc-T2^{ECFP} (Storrie *et al.*, 1998) or ARFGAP1^{EGFP} (Elsner *et al.*, 2003) grown in MatTek dishes (MatTek, Ashland, MA) were imaged using an Axiovert 200/LSM 510 META system (Carl Zeiss, Oberkochen, Germany) fitted with a water-corrected 40× Apochromat 1.2 NA objective and a humidified chamber with a constant temperature of 37°C and 5% CO_2 (CTI-Controller 3700 connected to Incubator S, Carl Zeiss). Cyan fluorescent protein (CFP) was excited with a 405-nm Blue diode laser, and the emitted fluorescence was captured through a 475-nm long-pass filter. For GFP, a 488-nm Argon laser was used and the emitted fluorescence was captured through a 505 to −530-nm band-pass filter. Fluorescence level was coded with a gray scale representing a pixel intensity of 25–255. For semi-quantitation, background fluorescence was subtracted. Images were analyzed using the Volocity Quantitation 4.1 software (Improvision, Software for Scientific Imaging, Coventry, United Kingdom).

For electron microscopy, cells were fixed using a double fixation protocol with osmium and tannic acid (Simionescu and Simionescu, 1976). Samples were dehydrated in graded ethanol series and embedded in Epon 812 (Serva, GTF, Gothenburg, Sweden). After 48 h at 60°C, ultrathin sections (60 nm) were cut and mounted on grids. Samples were examined on a LEO 912 OMEGA (energy filter transmission electron microscope, Zeiss) at 120 kV accelerating voltage. Digital images were obtained through a side-mounted MegaView III TEM CCD camera (Zeiss).

Stereology was performed essentially as described earlier (Misteli and Warren, 1995). Briefly, Golgi areas were defined as a Golgi stack with associated vesicular and tubular profiles including intercisternal space but not intervesicular, cytoplasmic space. Stacked cisternae comprised two or more cisternal profiles separated by a gap of 15 nm or less and overlapping by more than half their cross-sectional length. Cisternae ranged from continuous to extensively fenestrated and were defined as membrane profiles with a length more than four times their width, the width being not more than 40 nm. Fenestrated cisternae were often wider and more translucent but could be distinguished from tubules by their fenestration. Tubules were defined as profiles with a length more than 1.5 times their width, the latter exceeding 40 nm. These were more undulating than cisternae and when branched, formed networks. Vesicular profiles had spherical or nearly spherical (length <1.5 times their width) profiles and were defined as being localized inside the Golgi zone of exclusion. In tangential thin sections, the absence of a translucent lumen served as a criterion for the classification of 50–75-nm peri-Golgi round profiles as vesicles. Open profiles such as broken cisternae were not included in the quantitation. All membrane profiles on an image were counted except clearly identifiable contaminants such a mitochondria, plasma membrane, or ER (which totaled <10% of all profiles). The length or width of each cisterna, tubule, or vesicle profile was measured with the Volocity Classification 4.1 software (Improvison).

Photoconversion was essentially performed as described (Grabenbauer *et al.*, 2005). Briefly, cells were washed with prewarmed calcium- and magnesium-free PBS, pH 7.4, and fixed for 30 min with prewarmed fixative containing 2% glutaraldehyde (25% stock solution; Merck, Stockholm, Sweden) and 2% sucrose (USB, Cleveland, OH) in PBS. After washing three times with PBS, samples were blocked with 100 mM glycine (Sigma-Aldrich) and 100 mM potassium cyanide (Merck, Stockholm) in PBS for 2 h followed by 40 min with 10 mg/ml sodium borohydrate (Sigma-Aldrich) in PBS. For photoconversion, samples were washed twice in Tris/HCl buffer, pH 7.4, followed by incubation in a freshly prepared and oxygen saturated solution of 1.5 mg/ml 3,3′-diaminobenzidine hexahydrate (DAB; Polysciences, Eppelheim, Germany) in Tris/HCl buffer, pH 7.4, at 10°C or below. To bleach, samples were illuminated with the appropriate filter settings for enhanced CFP (ECFP;

excitation filter BP436/20) using a 100 W mercury lamp (FluoArc by Carl Zeiss). After photoconversion, samples were washed with distilled water and postfixed for 30 min on ice in 1% osmium tetroxide reduced by 1.5% potassium ferrocyanide. Samples were dehydrated in graded ethanol series and embedded in Epon 812 (Serva). After 48 h of polymerization, the glass bottom of the tissue culture dish was removed by hydrofluoric acid. Ultrathin sections (60 nm) of flat embedded cells were cut parallel to the surface on a Leica Ultracut S ultramicrotome (Leica, Bensheim, Germany) and mounted on Formvar coated grids.

For tomography, semithick sections (150 nm) of resin-embedded cells were prepared by microtomy and collected on copper grids covered with a carbon-coated pioloform layer. The sections were poststained in uranyl acetate and lead citrate. As fiducial markers for tomography, 10-nm colloidal gold particles were applied on top of the sections. Several tilt series were collected for each condition in a 120-kV Tecnai electron microscope (FEI Company, Eindhoven, The Netherlands), equipped with a 4K × 4K Eagle CCD camera (FEI Company). The tilt series covered an angular range of 130–140° around two orthogonal axes (Penczek *et al.,* 1995) sampled in 1° increments. The typical pixel size was 0.6 nm at the specimen level.

Processing of the tilt series was carried out with IMOD software package (Kremer *et al.,* 1996). Mutual alignment of the images in the tilt series was performed using the fiducial gold markers on top of the sample. Independent local alignment of 5 × 5 overlapping patches showed a reduction of the residual error mean by a factor of ~2 and was therefore applied to the data. The tomograms were then computed from the aligned tilt series by weighted back projection. The two tomograms obtained for each field of view from orthogonal tilt series were finally combined into a single reconstruction in IMOD (Mastronarde, 1997).

RESULTS

PA-derived DAG Is Rapidly Turned over in Golgi Membranes

proPr has been used previously to highlight the importance of DAG in the recruitment of proteins that contain the DAG-binding domain, C1, to membranes (Carrasco and Merida, 2004, 2007). For example, PKD has been shown to rapidly dissociate from *trans*-Golgi membranes in the presence of 500 μM proPr for 5 min (Baron and Malhotra, 2002). In that study, the conversion from PA into DAG was tested using proPr and was compared with conversion of PC and sphingomyelin into ceramide and DAG through ceramide synthase using fumonicin B1 at 25 μg/ml for 24 h. Both inhibitors caused PKD dissociation from the *trans*-Golgi. Other proteins are also likely to show preference for DAG. Even though the GTPase-activating protein, ARFGAP1, lacks a defined C1 domain, its binding and activity on liposomes is enhanced upon inclusion of DAG (Antonny *et al.,* 1997). The reason for such stimulation is not fully understood but is presumably due to a protein-lipid–induced conformational change facilitated by DAG (Mesmin *et al.,* 2007). Alternatively, membranes containing DAG have a higher propensity to form curved membranes (Shemesh *et al.,* 2003) thereby, potentially, stimulating activity. ARFGAP1 binding to Golgi membranes is also enhanced by DAG, in vivo, as evidenced by the addition of proPr to living cells. After 5 min, this resulted in a significant loss (~50%) from the Golgi apparatus of an overexpressed ARFGAP1 protein fused to the enhanced GFP (EGFP; Fernandez-Ulibarri *et al.,* 2007). This suggests that PA is continuously converted into DAG through the enzymatic activity of a PAP and that this is required for efficient ARFGAP1 binding to Golgi membranes.

We first tested which type of PAP was responsible for the PA-to-DAG conversion relevant to ARFGAP binding to Golgi membranes, in vitro. There are two types of PAPs: PAP1, which is cytosolic, and PAP2, which is membrane bound (for review, see Nanjundan and Possmayer, 2003). To distinguish between PAP1 and PAP2, we monitored the effect of proPr on the binding of recombinant HIS-tagged ARFGAP1 to purified Golgi in the presence or absence of cytosol. Figure 1A shows that the binding of recombinant and His-tagged ARFGAP1 to purified Golgi membranes is enhanced by the addition of cytosol. Addition of proPr effectively abolishes the promoting activity of the cytosol consistent with a cytosolic PAP. A lower, yet significant increase in ARFGAP1 binding was also observed upon addition of proPr in the absence of cytosol. This was contrary to what would be expected and at present, and we cannot offer a good explanation. Instead, we focused on the proPr-sensitive activity of the cytosol that promotes ARFGAP1 binding to Golgi membranes. The inhibition of DAG synthesis under proPr conditions was examined by measuring the amount of ^{32}P-PA after addition of cytosol. As shown in Supplementary Figure S1A, addition of proPr to purified rat liver Golgi membranes resulted only in a minor increase of ^{32}P-PA levels. An explanation for this can be that PA is still formed from, for example, PC or DAG. Addition of cytosol results in a significant increase in PA levels consistent with cytosolic factors stimulating PA synthesis. The stimulating effect of cytosol is greatly enhanced upon addition of proPr consistent with a rapid conversion of PA to DAG under normal conditions. When this step is blocked, PA accumulates as a consequence.

The ability of cytosol to promote ARFGAP1 binding to membranes and the sensitivity for proPr was tested next. In Supplementary Figure S1B, increasing amounts of proPr were added to the cytosol and as can be seen, a significant reduction in binding was observed at 300 μM. At higher concentrations, we did not observe any further decrease (data not shown). The cytosolic proPr-sensitive activity that promoted ARFGAP1 binding to Golgi membranes was further characterized through fractionation using ammonium sulfate, gel filtration, and ion exchange chromatography (outlined in Supplementary Figure S1C). This yielded an enriched proPr-sensitive fraction that was further analyzed by mass spectrometry. Among the 100 proteins identified, no peptides were detected from proteins relevant to COPI function (e.g., coatomer subunits, ARF proteins, or ARFGAPs). Taken together, the cytosolic and proPr-sensitive activity most likely corresponds to PAP1 though further characterization of the enriched fraction, and identification of the activity is required before any firm conclusions as to the nature of the relevant PAP can be drawn.

We also confirmed that ARFGAP1 binding to Golgi membranes is affected by the inhibition of PA-DAG conversion, in vivo, as observed by Egea and colleagues using overexpressed ARFGAP1 fused to EGFP (Fernandez-Ulibarri *et al.,* 2007). The use of 60 μM proPr in the Egea study, however, is unlikely to inhibit PAP1 completely because this enzyme requires at least 250 μM of proPr to be fully inhibited (judged by the resulting increase of cellular PA levels; Meier *et al.,* 1998). To test if ARFGAP1 is affected differently at higher concentrations of proPr, in vivo, we monitored the effect of 60 μM proPr on HeLa cells stably expressing ARFGAP1 fused to EGFP (ARFGAP1^{EGFP}; Elsner *et al.,* 2003) and compared this to 300 μM proPr. Figure 1, B–F, shows that the effect of 60 μM proPr on ARFGAP1^{EGFP} is only partial as compared with 300 μM. Even after 10 min, more than 25% of ARFGAP1^{EGFP} (Figure 1, B–D) remained on the Golgi apparatus in the presence of 60 μM, whereas at 300 μM, most if not all ARFGAP1^{EGFP} already had been lost after 20 s (Figure 1, B, E, and F). At 20 s, we observed no detectable loss of ARFGAP1^{EGFP} in the presence of 60 μM proPr or at 4°C for 10 min in the presence of 300 μM proPr (data not shown).

A rapid dissociation of ARFGAP1^{EGFP} from Golgi membranes in the presence of 300 μM proPr suggests that the half-life of PA-derived DAG is very short. To exclude that the rapid dissociation was not due to overexpression of an

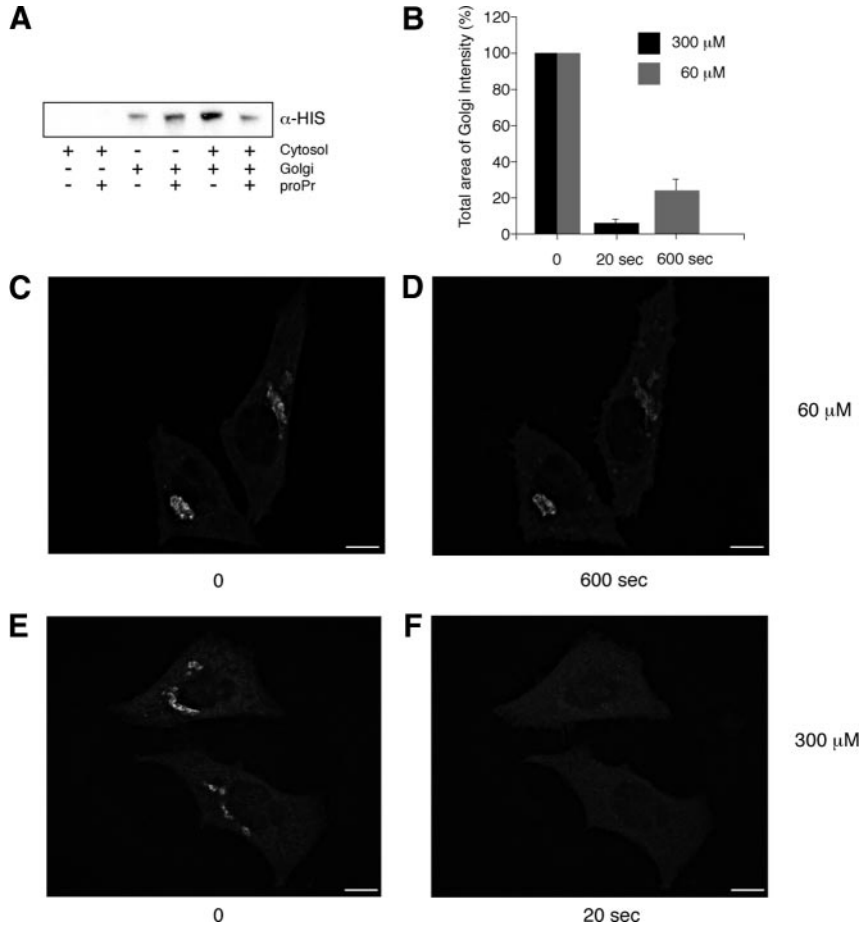

Figure 1. Inhibition of DAG formation through PAP1 results in a rapid loss of ARFGAP1 from Golgi membranes. (A) Inhibition of ARFGAP1 binding to Golgi membranes by proPr is cytosol-dependent. Recombinant His-tagged ARFGAP1 (0.1 μg) was incubated in 200 μl reaction buffer (see *Material and Methods*) together with highly purified Golgi membranes (20 μg), rat liver cytosol (1 mg), or proPr (300 μM) for 15 min at 37°C. Incubation mixtures were terminated on ice and membranes pelleted at 13 000 rpm for 10 min. Solubilized proteins were then separated by SDS-PAGE and transferred to nitrocellulose for Western blotting. His-ARFGAP1 was detected using a poly-His specific antibody followed by secondary HRP-labeled rabbit anti-mouse antibody and an ECL detection system. (B–F) Addition of 60 μM proPr for 600 s (C and D) or 300 μM proPr for 20 s in HeLa cells expressing ARFGAP1^{EGFP} (E and F), respectively, results in a partial or complete loss of the Golgi-localized ARFGAP1^{EGFP}. (B) Quantitation (abscissa) as described in *Materials and Methods.* Scale bars, (C–F) 10 μm.

EGFP fusion protein, we confirmed the loss of endogenous ARFGAP1 from the juxta-nuclear Golgi area in response to PAP inhibition by proPr. As shown in Supplementary Figure S2, most if not all Golgi-associated ARFGAP1 had redistributed to the cytosol after 3 min (compare Supplementary Figure S2, A with B). We also examined cells after shorter incubation times (i.e., 20 s) and found that most of the endogenous ARFGAP1 was lost from the Golgi area in less than a minute (data not shown). In the presence of proPr, endogenous COPI coatomer (revealed by antibodies to βCOP) remained largely unaffected (compare Supplementary Figure S2, D with E). After removal of the PAP inhibitor, ARFGAP1 was recruited back to the juxta-nuclear Golgi area within 2 min (Supplementary Figure S2C). As an independent control for DAG under these conditions, we also monitored the behavior of a mouse PKD mutant, $^{K}618_{N}$, fused to glutathione *S*-transferase, which is deficient in its kinase activity but still depends on DAG for its binding to the Golgi apparatus. As can be seen, expression of the PKD mutant resulted in the formation of tubules emanating from the Golgi (Supplementary Figure S2, G and I) as observed previously (Liljedahl *et al.*, 2001; Fernandez-Ulibarri *et al.*, 2007). On addition of proPr (300 μM) for 3 min, most if not all of the fusion protein had distributed to the cytosol (Supplementary Figure S2, H and J), showing that under these conditions DAG synthesis is fully inhibited. In respect to the behavior of ARFGAP1, we observed no difference between the D-or the L-form of proPr (data not shown). This ruled out the β-adrenergic receptor or, signaling through this receptor, as a cause for the observed effect. As proPr was dissolved in water and diluted more than 30 times before each experiment, additional vehicle experiments were deemed unnecessary.

PA-to-DAG Conversion Is Required for Bud Formation

The loss of ARFGAP1 but not coatomer suggests a partial impairment of COPI function. This is consistent with the observed inhibition of Golgi to ER recycling upon addition of proPr (Fernandez-Ulibarri *et al.*, 2007). In that study, loss of Golgi to ER recycling was explained by the concurrent 50% decrease of ARFGAP1 from the Golgi apparatus. Because ARFGAP1 has been implicated in the formation of COPI transport intermediates at the stage of membrane fission, such a decrease should impair the late stage of the budding process, i.e., membrane fission. Indeed, addition of 60 μM proPr for 15 min results in the accumulation of multiple membrane buds consistent with this interpretation (Fernandez-Ulibarri *et al.*, 2007). To investigate how proPr affects the Golgi cisternae at the higher concentration of 300 μM, we examined HeLa cells at the ultrastructural level using ultrathin plastic sections. Cells were incubated with 300 μM proPr for 3 min. In untreated cells, Golgi stacks were typically aligned laterally as part of the Golgi ribbon (Figure 2A). At higher magnification, a number of membrane buds and vesicular/tubular profiles (VTPs) could be seen in close proximity to the cisternal membranes of each Golgi stack (Figure 2D). Addition of proPr for 3 min resulted in an increased frequency of curved stacks with smooth cisternal membranes seemingly devoid of both membrane buds as well as VTPs (Figure 2,B and E, and Supplementary Figure

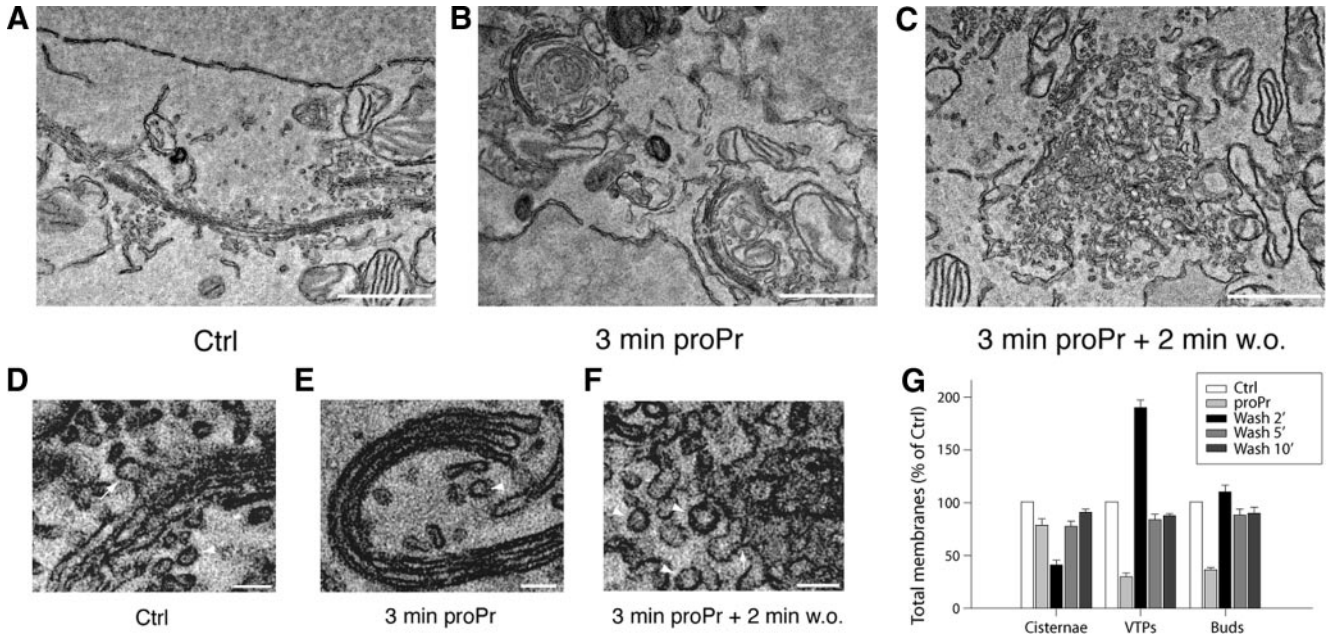

Figure 2. DAG is required for bud formation. Thin plastic embedded sections (60 nm thick) of HeLa cells were examined at the ultrastructural level. (A–C) Representative low-magnification fields (scale bar, 1 μm), whereas D–G show representative high-magnification fields (scale bar, 100 nm). (A and D) Multiple Golgi stacks align laterally to form a part of the Golgi ribbon in untreated cells. Associated membrane buds (arrow) and VTPs (arrowhead) were seen in close proximity to cisternal membranes of the Golgi stack. (B and E) Addition of 300 μM proPr for 3 min resulted in an increased frequency of curved stacks that consisted of smooth cisternal membranes seemingly devoid of both membrane buds as well as VTPs. Occasional VTPs and buds (arrowhead in E) were observed but at a marked decreased frequency (see G for quantitation). In C and F, removal of proPr resulted in a dramatic increase of both membrane buds as well as VTPs already after 2 min. Arrow and arrowheads point to a bud and VTPs, respectively. (G) Quantitation of cisternae, VTPs, and membrane buds presented as the mean of total membranes and compared with untreated control (Ctrl), which was set at 100%.

S3A). This observation was in strong contrast to that seen in HeLa cells incubated at the suboptimal concentration of 60 μM for 15 min. In such cells, Golgi areas had an increased frequency of both membrane buds as well as VTPs (Supplementary Figure S3B). Thus, at concentrations expected to fully block PAP1 activity, bud formation appears inhibited suggesting a role for DAG at this early stage of vesicle and tubule formation. At this higher concentration, we observed no discernable effects on other membrane systems, including mitochondria (see Supplementary Figure S3, E and F), and cells showed no loss of viability after removal of proPr (data not shown). At suboptimal concentrations, bud formation is not inhibited as are later stages of vesicle and tubule formation. Strikingly, removal of proPr, allowing DAG synthesis after 3-min incubation, resulted in a dramatic increase of cisternal buds as well as VTPs already after 2 min. As shown in Figure 2, C and F, this often resulted in Golgi areas with a reduced stack-like appearance. At 5–10 min after removal of proPr, however, the number of cisternae increased, whereas associated membrane buds and VTPs decreased approaching levels to that observed in control cells (see Figure 2G for quantitation and Supplementary Figure S3, C and D, for low-magnification fields). This suggests a rapid conversion of PA into DAG and that the latter is required at early stages of vesicle and tubule formation, i.e., for bud formation.

That membrane buds and associated VTPs are affected by proPr was confirmed by electron microscopy–based tomography of thick plastic sections. Representative tomograms of Golgi areas from control cells (Figure 3A, left panel), cells incubated with proPr for 3 min (Figure 3A, middle panel) and cells incubated with proPr for 3 min followed by a 2 min incubation after proPr removal (Figure 3A, right panel), revealed differences in the number of associated buds (yellow) as well as adjacent vesicles (red) and tubules (green), consistent with that observed and quantified using thin sections above. Quantitative tomography would require an examination of a large number of tomograms and is considered outside the scope of this study. Round-to-oval structures were labeled as vesicles if they maintained their X-Y position while moving up and down (along the Z-axis) in the tomogram and had a clearly defined top and bottom, i.e., they should appear and then disappear when moving up and down along the Z-axis. Structures were labeled as tubules if they had no defined top and bottom and moved in the X-Y direction when moving up and down along the Z-axis. At higher magnification, a fuzzy coat consistent with that of COPI (Orci *et al.*, 1986) was observed on buds and vesicles 2 min after removal of proPr (Figure 3B). Some membrane buds also had an electron-dense region bridging the constricted neck region (Figure 3B, arrows), consistent with a protein–lipid-aided fission machinery.

We next examined whether membrane buds and VTPs that form in response to proPr removal contain Golgi-resident enzymes. We examined HeLa cells stably expressing *N*-acetylgalactoseamine transferase-2 fused to the ECFP (GalNAcT2^{CFP}). We showed previously that if illuminated after fixation, GalNAcT2^{CFP} yields sufficient amounts of free radicals to precipitate DAB both locally as well as quantitatively (Grabenbauer *et al.*, 2005). As can be seen in Figure 4A, a gradient-like distribution of GalNAcT2^{CFP} was observed across Golgi stacks under normal conditions. Some associated VTPs were filled with DAB products consistent with the notion that GalNAcT2^{CFP} is capable of gaining access to these structures (Grabenbauer *et al.*, 2005). On addition of proPr during 3 min, the DAB precipitate was seen exclu-

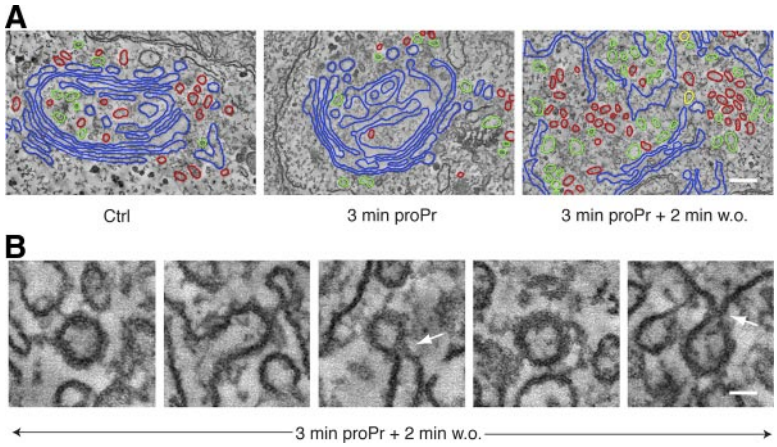

Figure 3. Electron tomography of Golgi stacks. Dual axis tomography was performed to obtain good resolution of membrane delineations in all specimen planes. (A) A digital slice through the 3D volume of an electron tomographic reconstruction illustrates the appearance of the Golgi area seen before addition of proPr (left field), 3 min after addition of proPr (middle field) and 2 min after removal of proPr (right field). Each membrane-delineated structure present in this digital slice was analyzed throughout the 3D volume and color-coded. Blue, Golgi cisterna or structures continuous with a Golgi cisterna except membrane buds; red, vesicles; green, tubular structures; and yellow, membrane buds. Scale bar, 100 nm. (B) Different close-up fields vesicles and membrane buds observed after removal of proPr. Arrows indicate necks of budding profiles that appear constricted by electron-dense material. Scale bar, 40 nm.

sively in cisternae (Figure 4B), whereas upon removal of proPr, the DAB precipitate was seen in both cisternal buds as well as VTPs (Figure 4, C and D). The diameter of observed VTPs were between 40 and 50 nm, consistent with the expected inner diameter of peri-Golgi COPI vesicles.

Taken together, the data presented so far suggests a direct requirement of PA-derived DAG for the formation of membrane buds and the resulting vesicles and tubules. Also, that the resident Golgi marker, GalNAcT2^{CFP} gains access to at least a part of formed structures. The rapid shifts in observed morphologies further indicate that underlying PA to DAG conversion takes place at a surprisingly high rate and that formed DAG has a relatively short half-life. This correlates well with the dissociation and rebinding of ARFGAP1 to Golgi membranes linking this ARFGAP to vesicle formation through DAG (Fernandez-Ulibarri *et al.*, 2007). In that study, Fernandez-Ulibarri, Egea and colleagues suggested that ARFGAP1 is required for the fission of membrane buds (vesicle budding). Having observed that inhibition of DAG synthesis prevents the formation of membrane buds, the early stage of vesicle and tubule formation, we here tested whether ARFGAP1 is required also for this step. Cells were either transfected with control interference RNA (RNAi^{Mock}) or interference RNA specific for ARFGAP1 (RNAi^{ARFGAP1}). At the ultrastructural level, RNAi^{Mock}-transfected cells revealed a somewhat higher incidence of associated VTPs and membrane buds that was similar to that observed in untransfected cells, suggesting some minor influence of the transfection procedure on the experiment (compare Figure 2A with Supplementary Figure S4A). In cells transfected with RNAi^{ARFGAP1}, there was a marked increase of membrane buds accompanied by a decreased number of associated VTPs compared with RNAi^{Mock}-transfected cells (Figure 5, A and D, and Supplementary Figure S4B) consistent with an impairment in vesicle fission as a consequence of lowering the endogenous ARFGAP1 protein level. As in untransfected cells (Figure 2), addition of proPr resulted in a marked decrease in associated membrane buds and VTPs in both RNAi^{Mock}-as well as RNAi^{ARFGAP1}-transfected cells (Figure 5, B and D, and Supplementary Figure S4, C and D). After 2 min of removal of proPr, cells transfected with RNAi^{ARFGAP1} revealed a dramatic increase in membrane buds compared with cells transfected with RNAi^{Mock} over that of associated VTPs (Figure 5, C and D, and Supplemen-

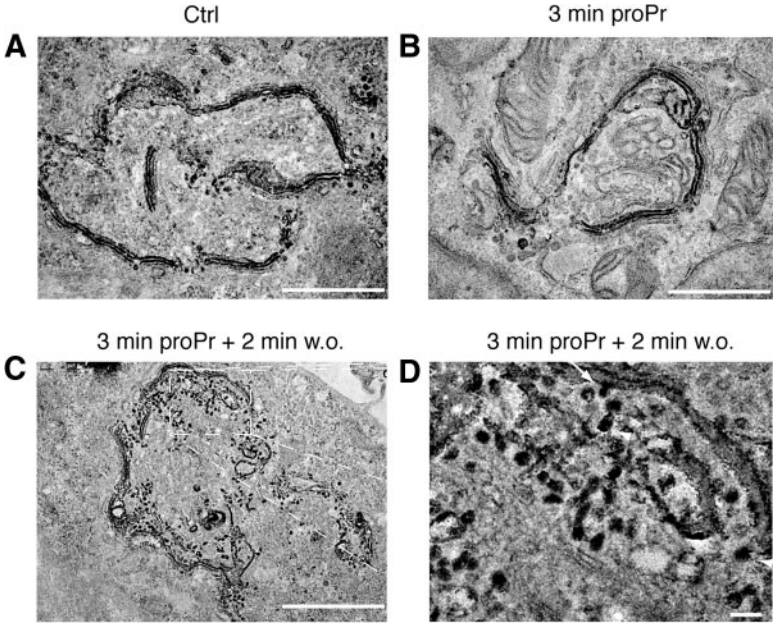

Figure 4. Inhibition of DAG formation prevents GalNAcT2^{CFP} from entering VTPs. After photooxidation and epon embedding, DAB precipitate was examined by electron microscopy. (A) DAB precipitate is predominantly found in 2–3 cisternae reflecting a gradient-like distribution across the Golgi stack. Some associated VTPs are also positive for the DAB precipitate, consistent with that GalNAcT2^{CFP} can gain access to these structures. (B) On addition of proPr (300 μM) for 3 min, the DAB precipitate is seen exclusively in cisternal membranes but cannot be detected in any associated buds or VTPs. (C) At 2 min after removal of proPr, the DAB product is seen in both cisternal membranes as well as VTPs. (D) Magnified field corresponding to the box in C. Arrow points to a bud-like structure filled with DAB precipitate. Arrowheads point to VTPs with a diameter of 40–50 nm. Scale bar, (A–C) 1 μm; (D) 75 nm.

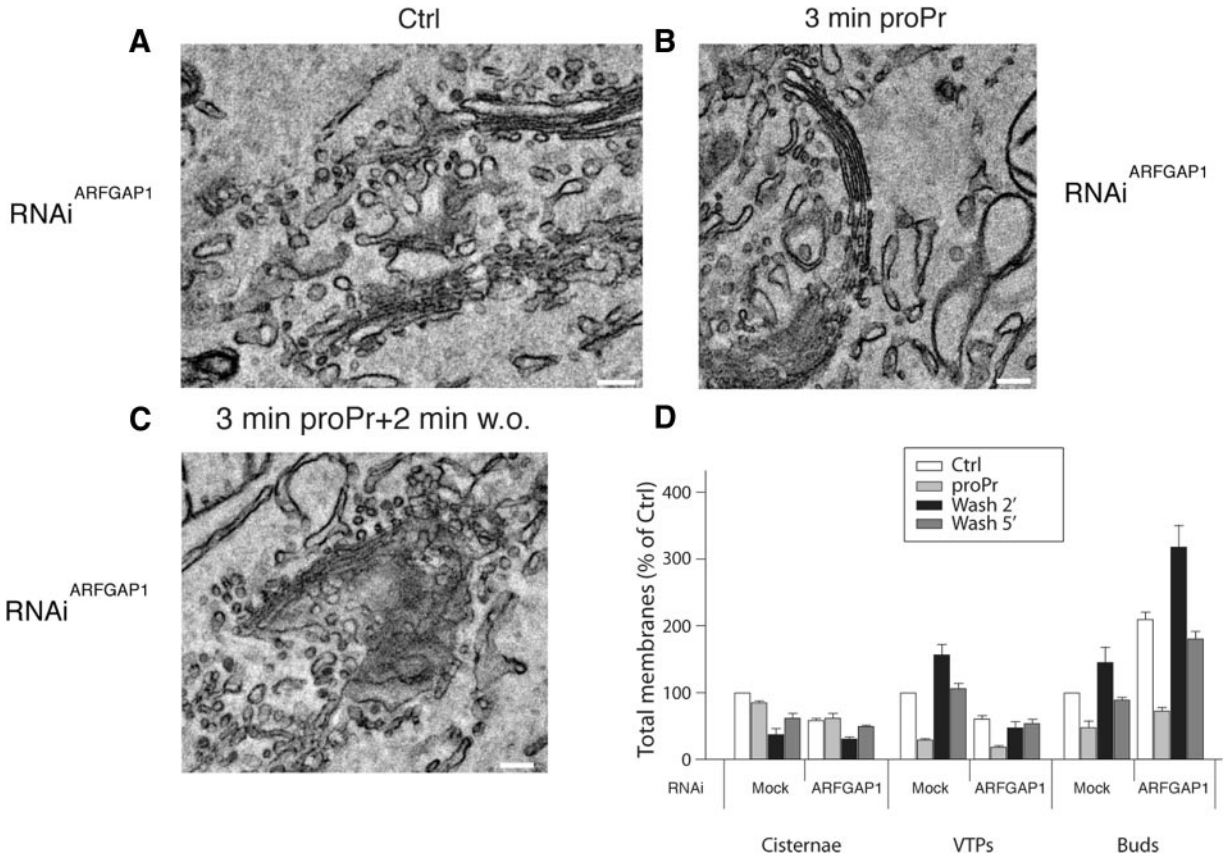

Figure 5. ARFGAP1 is required for membrane fission. Thin plastic embedded sections (60 nm thick) of HeLa cells transfected with either RNAi^{Mock} or RNAi^{ARFGAP1} were examined at the ultrastructural level to discern structures associated with Golgi stacks. Observed structures were quantified in D as in Figure 2. (A and D) RNAi^{ARFGAP1}-transfected cells revealed an increased frequency of membrane buds accompanied by a decreased number of associated VTPs compared with RNAi^{Mock}-transfected cells. (B and D) Addition of proPr (300 μM) for 3 min resulted in a marked decrease in associated membrane buds and VTPs in RNAi^{ARFGAP1}-transfected cells. (C and D) Removal of proPr revealed a marked increase in membrane buds in cells transfected with RNAi^{ARFGAP1} compared with cells transfected with RNAi^{Mock} over that of associated VTPs. Scale bar, 100 nm.

tary Figure S4, E and F). This shows that knockdown of ARFGAP1 results in a lowered ability to complete the budding process (presumably at the level of membrane fission or scission) because in such cells, the number of stack-associated VTPs was significantly lower than that of mock-transfected cells (Figure 5D). After 5 min of proPr removal, RNAi^{ARFGAP1}-transfected cells revealed ratios of VTPs and buds similar to that of cells not treated with proPr (Ctrl).

That endogenous ARFGAP1 had been knocked down was tested for by Western blotting of transfected cells. As shown in Supplementary Figure 5A, endogenous ARFGAP1 levels were diminished in cells transfected with RNAi^{ARFGAP1}, compared with cells transfected with RNAi^{Mock}. The introduction of RNAi^{ARFGAP1} did not cause nonspecific effects in addition to the knockdown of ARFGAP1, as shown by using RNAi derived from a scrambled sequence. Transfection with such RNAi, like the RNAi to GFP, did not result in any discernable differences compared to those presented and quantified in Figure 5. We also tested whether expression of rat ARFGAP fused to enhanced yellow fluorescent protein (EYFP) could overcome the phenotype observed in RNAi^{ARFGAP1}-transfected cells. Endogenous ARFGAP1 was knocked down, whereas expressed rat ARFGAP1^{EYFP} was unaffected by RNAi^{ARFGAP1}. Similar to previous observations, overexpression of ARFGAP1^{EYFP} resulted in loss of juxta-nuclear staining of Golgi enzymes (Aoe *et al.*, 1997; data not shown). At the ultrastructural level, we detected clusters of vesicles in those cells that expressed ARFGAP1^{EYFP} rather than Golgi cisternae with associated buds (Supplementary Figure S5D.). On the basis of this, we conclude that ARFGAP1 is unlikely to have a role in bud formation because the knockdown of endogenous ARFGAP1 resulted in an accumulation of buds. Instead, ARFGAP1 is most likely required for later stages in vesicle and tubule formation. This is separate from the role of DAG in the early stages of bud formation highlighted in this article.

DISCUSSION

We have presented evidence showing that synthesis of DAG from PA is required for bud formation in the Golgi apparatus and that ARFGAP1 promotes vesicle and tubule formation, presumably at the level of scission (summarized schematically in Figure 6A). We distinguished between a role for ARFGAP1 in vesicle and tubule formation compared with bud formation through the use of RNAi. Knockdown of endogenous ARFGAP1 resulted in a marked decrease in VTPs, consistent with a role for ARFGAP1 at the level of membrane scission (Yang *et al.*, 2005; Fernandez-Ulibarri *et al.*, 2007). Instead, we observed a marked increase of mem-

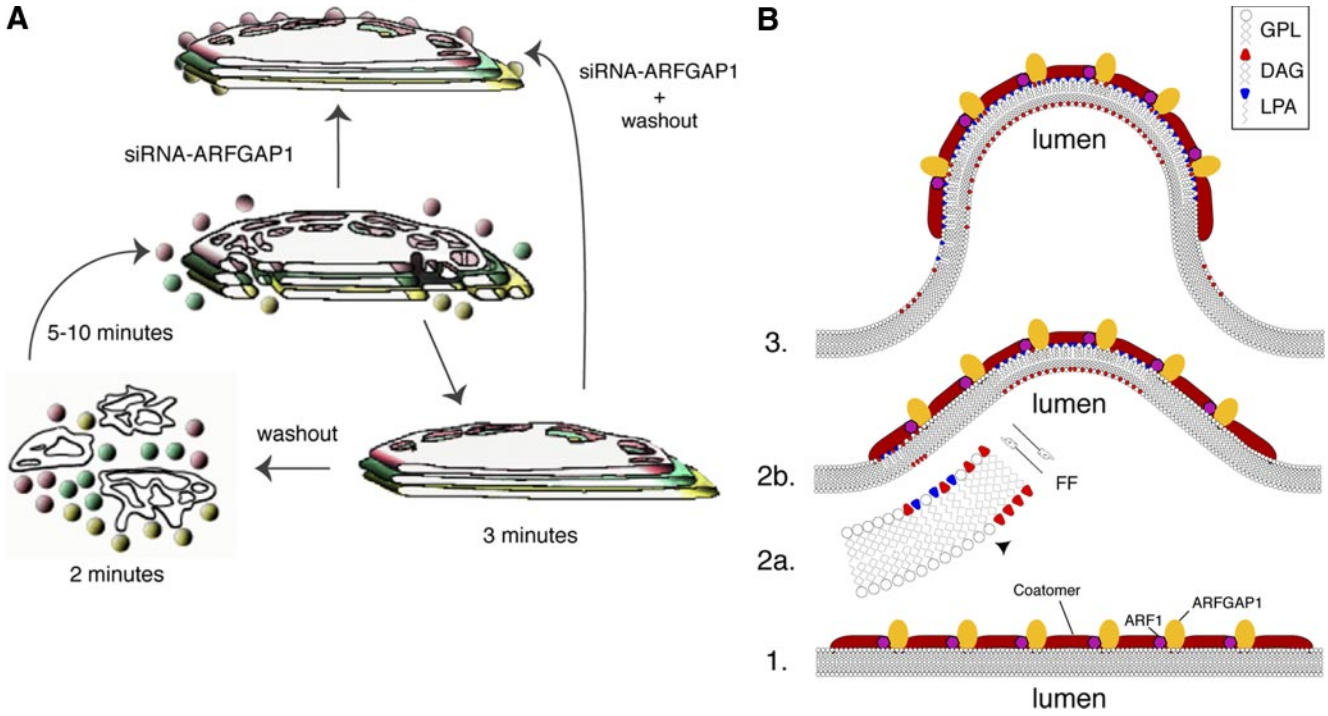

Figure 6. Schematic overview and model. (A) Inhibition of DAG synthesis in the Golgi results in an inhibition of bud formation after incubation with 300 μM proPr for 3 min. Observed Golgi stacks lack definable bud structures as well as adjacent vesicles and tubules and instead appear smooth and nonfenestrated compared with untreated cells. Resumption of DAG synthesis results in a rapid increase in bud, vesicle, and tubular formation already after 2 min. At 5–10 min after washout, stacks have reformed. This reveals an underlying rapid and dynamic behavior of Golgi membranes in response to DAG synthesis. Knockdown of ARFGAP1 through siRNA experiments results in Golgi stacks with associated buds but no adjacent vesicles and tubules. In such cells, addition of proPr for 3 min results in Golgi stacks devoid of buds. Taken together, this suggests a role for DAG in bud formation and a role for ARFGAP1 in later stages of vesicle and tubule formation (e.g., to promote vesicle scission). (B) A model illustrates the proposed function of DAG in terms of promoting bud formation. (1) COPI coat-components such as coatomer, ARF1, and ARFGAP1 bind to the cytosolic leaflet of the Golgi-cisternal membrane. (2a) Formation of LPA (an inverted cone-shaped lipid, depicted in blue) and DAG (a cone-shaped lipid, depicted in red), allows the membrane to bend outward (2b) into the cytosol. The ability of DAG to rapidly flip-flop (FF) over to the luminal leaflet explains why DAG is required for bud formation in its ability to promote negative curvature. (3) The bud has formed with LPA enriched in the cytosolic leaflet at the tip with DAG in the opposite luminal leaflet. At the base of the bud, PA- and DAG-binding proteins are proposed to help stabilize the intermediate. As DAG can easily flip-flop back to the cytosolic leaflet, it has been suggested that its presence causes disorder in the membrane and as a consequent results in an increased ability of ARFGAP1 to promote GTP-hydrolysis of ARF1 resulting in a loss of coatomer once the vesicle has been formed and released (scission). Note that LPA can be converted back into PA and used to form DAG. Equally well, DAG can be converted back to PA, which then can be used to for LPA. How this is regulated to promote COPI vesicle formation is presently unknown. GPL, general phospholipid.

brane buds. Again, addition of proPr for 2 min to such cells decreased the occurrence of membrane buds. These then reappeared after 2 min of removal of proPr but did not result in associated VTPs (Figure 5D, compare black bars between RNAi^{Mock} and RNAi^{ARFGAP1} in terms of VTPs and buds). The most simple explanation for this is that DAG plays a role in the early stages of bud formation and that ARFGAP1 is required for later events such as membrane scission through, for example, CtBP/Bars-50 (Yang *et al.*, 2005, 2006) and uncoating through the stimulation of GTP hydrolysis by ARF.

We also monitored the distribution of GalNAcT2^{CFP}. Under normal conditions, this fusion protein resids in two cisternae of the Golgi stack and in adjacent VTPs, some corresponding to vesicles (Grabenbauer *et al.*, 2005). On addition of proPr, such GalNAcT2^{CFP}-filled VTPs were absent (Figure 4B). In contrast, when removing proPr to restore DAG synthesis, the frequency of VTPs increased, and often such VTPs contained GalNAcT2^{CFP}, as inferred from quantitative GFP excitation-induced DAB precipitation (Grabenbauer *et al.*, 2005). After 5–10 min, the number of VTPs was comparable to those seen under normal conditions.

We specifically targeted the conversion of PA to DAG using the pharmacological drug, proPr. This allowed us to monitor rapid events that took place within minutes upon the addition and subsequent removal of proPr (see Figure 6A). Other pharmacological agents such as brefeldin A (BFA) have proven indispensable in elucidating dynamic aspects of the Golgi apparatus (Sciaky *et al.*, 1997) through its specific inhibition of COPI function by the ARF1 exchange factor GBF1 (Niu *et al.*, 2005). For proPr, there are two types of PAPs to consider as known targets (for review, see Nanjundan and Possmayer, 2003). The first is cytosolic and is termed PAP1. This enzyme has not yet been identified but appears to be recruited to microsomal membranes, at least in vitro (Martin-Sanz *et al.*, 1984). The second enzyme, PAP2, has been identified and extensively characterized and is incorporated into cellular membranes (mainly the plasma membrane) via multiple transmembrane domains. Both PAP1 and PAP2 are effectively inhibited by proPr. At present, we cannot make a formal distinction between PAP1 and PAP2 in terms of bud formation in the Golgi apparatus though the in vitro binding study presented in Figure 1A and Supplementary

Figure S1, which supports a role for PAP1. Candidate enzymes for PAP1 are possibly the lipins (for review, see Carman and Han, 2006), and future testing and characterization of the enriched cytosolic fraction shown in Supplementary Figure 1C should reveal the identity of which PAP is responsible for bud formation in the Golgi apparatus.

We find it unlikely that proPr affects ARFGAP1 directly because in the absence of cytosol, we observed an increased binding to Golgi membranes. Had proPr affected ARFGAP1 directly, such binding should not be expected. Furthermore, $RNAi^{ARFGAP1}$-transfected cells were still capable of bud formation and still responded to proPr. Hence, it is improbable that ARFGAP1 is a direct target for proPr. Similarly, we find it unlikely that coatomer is a target of proPr because its binding to Golgi membranes was not affected by proPr (Supplementary Figure 2, D and E). We also monitored ARF1 expressed as an EGFP-fusion protein and found that it was not lost from the Golgi apparatus upon proPr addition (data not shown). The presence or absence of coatomer on Golgi membranes is nevertheless not predicted to inhibit bud formation. Loss of coatomer from Golgi membranes upon BFA addition results in extensive tubule formation. The opposite, recruitment of coatomer under conditions where GTP hydrolysis by ARF1 is inhibited, results in vesicle formation (e.g., upon addition of nonhydrolyzable analogues of GTP or the constitutively active mutant of ARF1, $^{Q}71_{L}$). In both cases, bud formation is a prerequisite that in the present study is inhibited upon addition of proPr. Thus, we find it unlikely that inhibition of COPI function could explain the observed decrease in bud formation. Rather, it is a lack of PA-derived DAG. DAG may also be generated in the Golgi through spingomyelin synthase activity. However this enzymatic activity is primarily localized in the *trans*-Golgi. Interfering with the synthesis of DAG through this pathway, using fumonisin B1 to inhibit ceramide synthetase to deprive sphingomyelin synthase from its substrate, had no effect on ARFGAP1 localization. Most likely, this is due to ARFGAP1's preference for DAG's having particular acyl chains, as shown in liposome-based experiments (Antonny *et al.*, 1997). It was found that ARFGAP1 had an increased activity when incubated with liposomes formed at a high DAG/PC ratio using DAG that contained two unsaturated oleyl chains. This pointed to a preference for DAG derived from the PC/LPA/PA pathway.

We were surprised by the rapid response of proPr in terms of bud and vesicle formation. At the concentration used (300 μM), PAP1 is expected to be fully inhibited (Meier *et al.*, 1998), consequently preventing conversion of PA into DAG (see Figure 6B). Because PA is cone-shaped, this lipid would promote negative curvature in the cytosolic leaflet, ensuring that buds can proceed through the latter stages by the closing of the neck region. Conversion of PA into DAG, also a cone-shaped lipid, would ensure that ARFGAP1 is recruited in order to aid in the fission/scission event (Yang *et al.*, 2005, 2006). Our finding that an inhibition of PA-to-DAG conversion results in a marked decrease in membrane buds suggests that also DAG is needed to promote membrane curvature at early stages of bud formation. We suggest, based on our observations, that an accumulation of PA is unfavorable for bud formation and that it is DAG that is required to form the bud (see Shemesh *et al.*, 2003 for theoretical modeling). We speculate that DAG can promote bud formation through its rather unique ability to flip-flop (within seconds; Bai and Pagano, 1997) across from the cytosolic leaflet to the luminal leaflet (see model presented in Figure 6B), promoting negative curvature on this side of the membrane. Because PA and other phospholipids flip-flop at a much slower rate (within minutes or hours), these have more defined roles on the cytosolic leaflet where, for example, LPA through its inverted cone-shape, will promote positive curvature.

Formation of COPI vesicles likely involves multiple steps. Initially, local fluctuations in membranes that occur naturally enable bud structures to form transiently (see Figure 6B). These are then stabilized by proteins such as coat proteins binding to the cytosolic surface of the membrane (see Reynwar *et al.*, 2007 and references therein). Such fluctuations are stimulated by the presence of membrane proteins (Kim *et al.*, 1998) as well as DAG, where the latter can flip-flop rapidly between the two leaflets. On the cytosolic leaflet, PA is also converted into LPA, which is an effective promoter of positive curvature. The coated buds can now form and proceed to vesicle scission with the help of ARFGAP1/ctBP/Bars-50 and acyl-CoA and other factors. As acyl-CoA is required for vesicle formation (Ostermann *et al.*, 1993; Yang *et al.*, 2005), it suggests that LPA is also needed as a source for PA and presumably also for DAG formation at the later stages of vesicle formation. An increase in DAG formation at this stage may also stimulate the GTPase-activating ability of ARFGAP1, resulting in uncoating of the vesicle once formed (Antonny *et al.*, 2005).

ACKNOWLEDGMENTS

We acknowledge Sjoerd van der Post at the Proteomics facility of the University of Gothenburg, Sweden, for help with initial characterization of cytosol fractions through mass spectrometry, Dr. David Mastronarde at the University of Colorado for his help and advise on tomographic reconstruction of 4K × 4K image stacks, Dr. Adrian C. Oprins (UMCU, Utrecht, The Netherlands) for graphics used in Figure 6A, and Yvonne Josefsson and Dr. Bengt R. Johansson at the Institute of Biomedicine, University of Gothenburg, Sweden, for preparation of thin sections and the use of the transmission microscope, respectively.

REFERENCES

Allan, V. J., and Kreis, T. E. (1986). A microtubule-binding protein associated with membranes of the Golgi apparatus. J. Cell Biol. *103*, 2229–2239.

Antonny, B., Bigay, J., Casella, J. F., Drin, G., Mesmin, B., and Gounon, P. (2005). Membrane curvature and the control of GTP hydrolysis in Arf1 during COPI vesicle formation. Biochem. Soc. Trans. *33*, 619–622.

Antonny, B., Huber, I., Paris, S., Chabre, M., and Cassel, D. (1997). Activation of ADP-ribosylation factor 1 GTPase-activating protein by phosphatidylcholine-derived diacylglycerols. J. Biol. Chem. *272*, 30848–30851.

Aoe, T., Cukierman, E., Lee, A., Cassel, D., Peters, P. J., and Hsu, V. W. (1997). The KDEL receptor, ERD2, regulates intracellular traffic by recruiting a GTPase-activating protein for ARF1. EMBO J. *16*, 7305–7316.

Bai, J., and Pagano, R. E. (1997). Measurement of spontaneous transfer and transbilayer movement of BODIPY-labeled lipids in lipid vesicles. Biochemistry *36*, 8840–8848.

Baron, C. L., and Malhotra, V. (2002). Role of diacylglycerol in PKD recruitment to the TGN and protein transport to the plasma membrane. Science *295*, 325–328.

Bethune, J., Wieland, F., and Moelleken, J. (2006). COPI-mediated transport. J. Membr. Biol. *211*, 65–79.

Brown, H. A., Gutowski, S., Kahn, R. A., and Sternweis, P. C. (1995). Partial purification and characterization of Arf-sensitive phospholipase D from porcine brain. J. Biol. Chem. *270*, 14935–14943.

Brown, H. A., Gutowski, S., Moomaw, C. R., Slaughter, C., and Sternweis, P. C. (1993). ADP-ribosylation factor, a small GTP-dependent regulatory protein, stimulates phospholipase D activity. Cell *75*, 1137–1144.

Carman, G. M., and Han, G. S. (2006). Roles of phosphatidate phosphatase enzymes in lipid metabolism. Trends Biochem. Sci. *31*, 694–699.

Carrasco, S., and Merida, I. (2004). Diacylglycerol-dependent binding recruits PKCtheta and RasGRP1 C1 domains to specific subcellular localizations in living T lymphocytes. Mol. Biol. Cell *15*, 2932–2942.

Carrasco, S., and Merida, I. (2007). Diacylglycerol, when simplicity becomes complex. Trends Biochem. Sci. *32*, 27–36.

Chen, Y. G., Siddhanta, A., Austin, C. D., Hammond, S. M., Sung, T. C., Frohman, M. A., Morris, A. J., and Shields, D. (1997). Phospholipase D stimulates release of nascent secretory vesicles from the trans-Golgi network. J. Cell Biol. *138*, 495–504.

Cockcroft, S., Thomas, G. M., Fensome, A., Geny, B., Cunningham, E., Gout, I., Hiles, I., Totty, N. F., Truong, O., and Hsuan, J. J. (1994). Phospholipase D: a downstream effector of ARF in granulocytes. Science *263*, 523–526.

Corda, D., Colanzi, A., and Luini, A. (2006). The multiple activities of CtBP/BARS proteins: the Golgi view. Trends Cell Biol. *16*, 167–173.

de Figueiredo, P., Drecktrah, D., Polizotto, R. S., Cole, N. B., Lippincott-Schwartz, J., and Brown, W. J. (2000). Phospholipase A2 antagonists inhibit constitutive retrograde membrane traffic to the endoplasmic reticulum. Traffic *1*, 504–511.

Dominguez, M., Dejgaard, K., Fullekrug, J., Dahan, S., Fazel, A., Paccaud, J. P., Thomas, D. Y., Bergeron, J. J., and Nilsson, T. (1998). gp25L/emp24/p24 protein family members of the cis-Golgi network bind both COP I and II coatomer. J. Cell Biol. *140*, 751–765.

Elsner, M., Hashimoto, H., Simpson, J. C., Cassel, D., Nilsson, T., and Weiss, M. (2003). Spatiotemporal dynamics of the COPI vesicle machinery. EMBO Rep. *4*, 1000–1004.

Fernandez-Ulibarri, I., Vilella, M., Lazaro-Dieguez, F., Sarri, E., Martinez, S. E., Jimenez, N., Claro, E., Merida, I., Burger, K. N., and Egea, G. (2007). Diacylglycerol is required for the formation of COPI vesicles in the Golgi-to-ER transport pathway. Mol. Biol. Cell *18*, 3250–3263.

Frigerio, G., Grimsey, N., Dale, M., Majoul, I., and Duden, R. (2007). Two human ARFGAPs associated with COP-I-coated vesicles. Traffic *8*, 1644–1655.

Gallop, J. L., Butler, P. J., and McMahon, H. T. (2005). Endophilin and CtBP/BARS are not acyl transferases in endocytosis or Golgi fission. Nature *438*, 675–678.

Grabenbauer, M., Geerts, W. J., Fernadez-Rodriguez, J., Hoenger, A., Koster, A. J., and Nilsson, T. (2005). Correlative microscopy and electron tomography of GFP through photooxidation. Nat. Methods *2*, 857–862.

Houle, M. G., Kahn, R. A., Naccache, P. H., and Bourgoin, S. (1995). ADP-ribosylation factor translocation correlates with potentiation of GTP gamma S-stimulated phospholipase D activity in membrane fractions of HL-60 cells. J. Biol. Chem. *270*, 22795–22800.

Huber, I., Rotman, M., Pick, E., Makler, V., Rothem, L., Cukierman, E., and Cassel, D. (2001). Expression, purification, and properties of ADP-ribosylation factor (ARF) GTPase activating protein-1. Methods Enzymol. *329*, 307–316.

Kim, K. S., Neu, J., and Oster, G. (1998). Curvature-mediated interactions between membrane proteins. Biophys. J. *75*, 2274–2291.

Kirchhausen, T. (2000). Three ways to make a vesicle. Nat. Rev. Mol. Cell Biol. *1*, 187–198.

Kremer, J. R., Mastronarde, D. N., and McIntosh, J. R. (1996). Computer visualization of three-dimensional image data using IMOD. J. Struct. Biol. *116*, 71–76.

Ktistakis, N. T., Brown, H. A., Sternweis, P. C., and Roth, M. G. (1995). Phospholipase D is present on Golgi-enriched membranes and its activation by ADP ribosylation factor is sensitive to brefeldin A. Proc. Natl. Acad. Sci. USA *92*, 4952–4956.

Ktistakis, N. T., Brown, H. A., Waters, M. G., Sternweis, P. C., and Roth, M. G. (1996). Evidence that phospholipase D mediates ADP ribosylation factor-dependent formation of Golgi coated vesicles. J. Cell Biol. *134*, 295–306.

Lanoix, J., Ouwendijk, J., Lin, C. C., Stark, A., Love, H. D., Ostermann, J., and Nilsson, T. (1999). GTP hydrolysis by arf-1 mediates sorting and concentration of Golgi resident enzymes into functional COP I vesicles. EMBO J. *18*, 4935–4948.

Lanoix, J., Ouwendijk, J., Stark, A., Szafer, E., Cassel, D., Dejgaard, K., Weiss, M., and Nilsson, T. (2001). Sorting of Golgi resident proteins into different subpopulations of COPI vesicles: a role for ArfGAP1. J. Cell Biol. *155*, 1199–1212.

Liljedahl, M., Maeda, Y., Colanzi, A., Ayala, I., Van Lint, J., and Malhotra, V. (2001). Protein kinase D regulates the fission of cell surface destined transport carriers from the trans-Golgi network. Cell *104*, 409–420.

Martin-Sanz, P., Hopewell, R., and Brindley, D. N. (1984). Long-chain fatty acids and their acyl-CoA esters cause the translocation of phosphatidate phosphohydrolase from the cytosolic to the microsomal fraction of rat liver. FEBS Lett. *175*, 284–288.

Mastronarde, D. N. (1997). Dual-axis tomography: an approach with alignment methods that preserve resolution. J. Struct. Biol. *120*, 343–352.

Meier, K. E., Gause, K. C., Wisehart-Johnson, A. E., Gore, A. C., Finley, E. L., Jones, L. G., Bradshaw, C. D., McNair, A. F., and Ella, K. M. (1998). Effects of propranolol on phosphatidate phosphohydrolase and mitogen-activated protein kinase activities in A7r5 vascular smooth muscle cells. Cell Signal. *10*, 415–426.

Mesmin, B., Drin, G., Levi, S., Rawet, M., Cassel, D., Bigay, J., and Antonny, B. (2007). Two lipid-packing sensor motifs contribute to the sensitivity of ArfGAP1 to membrane curvature. Biochemistry *46*, 1779–1790.

Misteli, T., and Warren, G. (1995). Mitotic disassembly of the Golgi apparatus in vivo. J. Cell Sci. *108*(Pt 7), 2715–2727.

Nanjundan, M., and Possmayer, F. (2003). Pulmonary phosphatidic acid phosphatase and lipid phosphate phosphohydrolase. Am. J. Physiol. Lung Cell Mol. Physiol. *284*, L1–L23.

Niu, T. K., Pfeifer, A. C., Lippincott-Schwartz, J., and Jackson, C. L. (2005). Dynamics of GBF1, a brefeldin A-sensitive Arf1 exchange factor at the Golgi. Mol. Biol. Cell *16*, 1213–1222.

Orci, L., Glick, B. S., and Rothman, J. E. (1986). A new type of coated vesicular carrier that appears not to contain clathrin: its possible role in protein transport within the Golgi stack. Cell *46*, 171–184.

Ostermann, J., Orci, L., Tani, K., Amherdt, M., Ravazzola, M., Elazar, Z., and Rothman, J. E. (1993). Stepwise assembly of functionally active transport vesicles. Cell *75*, 1015–1025.

Palmer, D. J., Helms, J. B., Beckers, C. J., Orci, L., and Rothman, J. E. (1993). Binding of coatomer to Golgi membranes requires ADP-ribosylation factor. J. Biol. Chem. *268*, 12083–12089.

Penczek, P., Marko, M., Buttle, K., and Frank, J. (1995). Double-tilt electron tomography. Ultramicroscopy *60*, 393–410.

Reinhard, C., Schweikert, M., Wieland, F. T., and Nickel, W. (2003). Functional reconstitution of COPI coat assembly and disassembly using chemically defined components. Proc. Natl. Acad. Sci. USA *100*, 8253–8257.

Reynwar, B. J., Illya, G., Harmandaris, V. A., Muller, M. M., Kremer, K., and Deserno, M. (2007). Aggregation and vesiculation of membrane proteins by curvature-mediated interactions. Nature *447*, 461–464.

Rivas, M. P., Kearns, B. G., Xie, Z., Guo, S., Sekar, M. C., Hosaka, K., Kagiwada, S., York, J. D., and Bankaitis, V. A. (1999). Pleiotropic alterations in lipid metabolism in yeast sac1 mutants: relationship to "bypass Sec14p" and inositol auxotrophy. Mol. Biol. Cell *10*, 2235–2250.

Roberts, R., Sciorra, V. A., and Morris, A. J. (1998). Human type 2 phosphatidic acid phosphohydrolases. Substrate specificity of the type 2a, 2b, and 2c enzymes and cell surface activity of the 2a isoform. J. Biol. Chem. *273*, 22059–22067.

Schmidt, A., Wolde, M., Thiele, C., Fest, W., Kratzin, H., Podtelejnikov, A. V., Witke, W., Huttner, W. B., and Soling, H. D. (1999). Endophilin I mediates synaptic vesicle formation by transfer of arachidonate to lysophosphatidic acid. Nature *401*, 133–141.

Sciaky, N., Presley, J., Smith, C., Zaal, K. J., Cole, N., Moreira, J. E., Terasaki, M., Siggia, E., and Lippincott-Schwartz, J. (1997). Golgi tubule traffic and the effects of brefeldin A visualized in living cells. J. Cell Biol. *139*, 1137–1155.

Shemesh, T., Luini, A., Malhotra, V., Burger, K. N., and Kozlov, M. M. (2003). Prefission constriction of Golgi tubular carriers driven by local lipid metabolism: a theoretical model. Biophys. J. *85*, 3813–3827.

Simionescu, N., and Simionescu, M. (1976). Galloylglucoses of low molecular weight as mordant in electron microscopy. I. Procedure and evidence for mordanting effect. J. Cell Biol. *70*, 608–621.

Sonoda, H., Okada, T., Jahangeer, S., and Nakamura, S. (2007). Requirement of phospholipase D for ilimaquinone-induced Golgi membrane fragmentation. J. Biol. Chem. *282*, 34085–34092.

Spang, A., Matsuoka, K., Hamamoto, S., Schekman, R., and Orci, L. (1998). Coatomer, Arf1p, and nucleotide are required to bud coat protein complex I-coated vesicles from large synthetic liposomes. Proc. Natl. Acad. Sci. USA *95*, 11199–11204.

Storrie, B., White, J., Rottger, S., Stelzer, E. H., Suganuma, T., and Nilsson, T. (1998). Recycling of golgi-resident glycosyltransferases through the ER reveals a novel pathway and provides an explanation for nocodazole-induced Golgi scattering. J. Cell Biol. *143*, 1505–1521.

Truett, A. P., 3rd, Bocckino, S. B., and Murray, J. J. (1992). Regulation of phosphatidic acid phosphohydrolase activity during stimulation of human polymorphonuclear leukocytes. FASEB J. *6*, 2720–2725.

Weigert, R. *et al.* (1999). CtBP/BARS induces fission of Golgi membranes by acylating lysophosphatidic acid. Nature *402*, 429–433.

Weiss, M., and Nilsson, T. (2003). A kinetic proof-reading mechanism for protein sorting. Traffic *4*, 65–73.

Yang, J. S. *et al.* (2008). A role for phosphatidic acid in COPI vesicle fission yields insights into Golgi maintenance. Nat. Cell Biol. *10*, 1146–1153.

Yang, J. S., Lee, S. Y., Spano, S., Gad, H., Zhang, L., Nie, Z., Bonazzi, M., Corda, D., Luini, A., and Hsu, V. W. (2005). A role for BARS at the fission step of COPI vesicle formation from Golgi membrane. EMBO J. *24*, 4133–4143.

Yang, J. S., Zhang, L., Lee, S. Y., Gad, H., Luini, A., and Hsu, V. W. (2006). Key components of the fission machinery are interchangeable. Nat. Cell Biol.